Rovibrational wave-packet manipulation using shaped midinfrared femtosecond pulses

Masaaki Tsubouchi,[1,3] Alexander Khramov,[2] and Takamasa Momose[1,2,3,*]

[1]*Department of Chemistry, The University of British Columbia, 2036 Main Mall, Vancouver, British Columbia, Canada V6T 1Z1*

[2]*Department of Physics and Astronomy, The University of British Columbia, 6224 Agricultural Road, Vancouver, British Columbia, Canada V6T 1Z1*

[3]*CREST, Japan Science and Technology Agency, Kawaguchi, Saitama, 332-0012, Japan*

(Received 15 August 2007; revised manuscript received 27 October 2007; published 5 February 2008)

We have calculated the propagation of rovibrational wave-packet in the $^1\Sigma$ state of CO and the $^2\Pi$ state of NO manipulated by shaped midinfrared femtosecond laser pulses. The rotational states of the molecules were fully taken into account in the calculation and the effects of the rotational states in the vibrational wave-packet evolution were examined in detail. As a result, it is found that rotational excitations associated with the vibrational excitation affect the wave-packet propagation drastically, which suggests that the rotational states should not be ignored when vibrational states of molecules are used as the target state for coherent control and qubits for quantum computation. For the experimental detection of the amplitude and phase information on the rovibrational wave-packets, the time profiles of the transition intensities from the rovibrational wave-packet to an electronically excited state were calculated. It is shown that both ionization and laser induced fluorescence signals contain information necessary for the analysis of the phase and relative amplitude of the rovibrational wave-packets.

DOI: 10.1103/PhysRevA.77.023405 PACS number(s): 37.10.Jk, 03.67.Lx, 03.67.Mn, 42.55.−f

I. INTRODUCTION

Wave-packet manipulation in molecules has been studied with great interest, especially for the control of the quantum system coherently. Coherent control of molecular systems has a capability of reaction control, quantum calculation, and so on [1–3]. Since the pioneering work by Scherer *et al.* [4], numbers of papers have been reported both experimentally [4–16] and theoretically [17–25]. Most of the experiments were done in the electronic excited states of molecules using femtosecond laser pulses.

Laser pulse shaping is a powerful method for the coherent control of molecular wave-packets. Warren has suggested theoretically that the arbitrary shaped laser pulse can be applied to control the population and coherence in the two-level systems [17], and examined the control of an I_2 excitation experimentally using a 100 ns laser pulse shaped by an acousto-optical modulator (AOM) [26]. Leone and co-workers have demonstrated the manipulation of the rovibrational wave-packet dynamics on the E state of Li_2 by using a femtosecond laser pulse shaped by a liquid crystal spatial light modulator (LC-SLM) [27]. They further extended this method to realize quantum gate operations [28,29] and the Deutsch-Jozsa algorithm [30]. Meanwhile, Judson and Rabitz suggested that the evolutional (genetic) algorithms can systematically optimize the shape of laser pulses to control molecular dynamics [31]. Warren and co-workers optimized the electronic population transfer of a dye molecule in solution by shaped pulses optimized by the genetic algorithm [32].

Studies of vibrational wave-packet in the electronic ground state have also been reported by several groups. Chirped midinfrared (MIR) pulses were used for the manipulation of the rovibrational wave-packet in the electronic ground state. Corkum and co-workers suggested that a chirped femtosecond infrared laser pulse can dissociate molecules efficiently in the electronic ground state *via* vibrational ladder climbing [22]. The vibrational ladder climbing enhanced by the negative chirp was observed for CO-stretching transitions of complex molecules in solution [33–36], and within gaseous NO molecule [37–39]. In order to manipulate the vibrational wave-packet more efficiently, arbitrary shaped MIR pulses are indispensable. Recently, the difference frequency mixing of shaped pulses using conventional pulse shapers in the visible and near IR region has been used to obtain arbitrary shaped MIR pulses [40–45]. Direct MIR pulse amplitude shaping has been achieved by placing a spectral filter into a grating pair by Weiner and co-workers [46]. Zanni and co-workers have demonstrated direct pulse shaping in both amplitude and phase using a germanium AOM [47,48].

One of the conceivable applications of rovibrational wave-packet manipulation in the electronic ground state is quantum computation. The decoherence time of rovibrational states in the ground electronic state is much longer than that in the excited electronic states, which is favorable especially for quantum gate operations. Vivid-Riedle and co-workers proposed that the normal modes of molecular vibrations can be used as qubits [49]. Quantum gate operations using shaped MIR light interacting with two vibrational normal modes have been examined theoretically for acetylene [50–54] and $MnBr(CO_5)$ [55]. Babikov also investigated quantum gate operations using OH molecules theoretically [56]. In these works, MIR pulse shapes were optimized by optimal control theory to realize quantum gates with high fidelity using pure vibrational states.

In order to realize molecular quantum computers using rovibrational states as qubits, one has to overcome essential issues such as realization of scalability as in the case of other

*momose@chem.ubc.ca

candidates. Nevertheless, it is still important to examine the implementation of elementary quantum gates onto rovibrational states in terms of fundamental understanding of interaction with radiation and molecules and future application to coherent control and manipulation.

In all the works so far reported, the effect of rotational states of molecules has been ignored completely. If one could use molecules in normal solids or liquids as qubits for quantum computation, rotational states might be ignored as any rotational motion is quenched in condensed phases. Extremely rapid dephasing, however, of rovibrational states of molecules in normal solids or liquids makes such application impractical. One should use molecules in the gas phase or in quantum solids [57,58] or liquids [59,60], in which vibrational dephasing is extremely long, for practical manipulation. In the gas phase as well as in quantum solids or liquids, rotational motion of molecules is well quantized, and rotational excitations occur inevitably together with vibrational excitations. Therefore, the effect of the rotational motion to the vibrational wave-packet propagation has to be examined carefully.

In this paper, we have examined vibration-rotation wave-packet manipulation in the electronic ground state using femtosecond MIR laser pulses. We explicitly included rotational states as well as vibrational states in the calculation as described in Sec. II. We focused on rovibrational wave-packets created by simple pulses, and wave-packet evolutions as a function of the intensity, pulse width, and chirp of shaped MIR laser pulses were examined in detail in order to clarify the effect of rotational motion in the wave-packet manipulation from an experimental point of view. Wave-packets manipulated by the double MIR pulses are also discussed by changing the separation and relative phase of pulse pairs. Wave-packet manipulation of more complicated pulses will be discussed in a separate paper [61].

To investigate the effect of the rotational motion, we have treated two different types of diatomic molecules. One is a CO molecule whose ground electronic state is $^1\Sigma^+$, and the other is a NO molecule whose ground electronic state is $^2\Pi_{1/2}$. Because of the difference in the electronic states and spin multiplicities, the wave-packet motion of NO is expected to be more complicated than that of a singlet CO molecule.

For the experimental observation of the wave-packet, the detection method of the phase and amplitude of wave-packets should be discussed. Laser induced fluorescence and resonance enhanced multiphoton ionization are widely used for the detection of the propagation of rovibrational wave-packets. Detection intensities of wave-packets are proportional to one-photon transition probability to an excited electronic state in these methods. Therefore, we have also examined the temporal evolution of the signal of the one-photon transition probability along with the wave-packet propagation in order to see how we could observe details of the wave-packet.

II. THEORY

In this section, we briefly describe the theoretical formalism for the calculation of the time a evolution of a rovibrational wave-packet manipulated by a shaped MIR pulse. For simplicity, Hamiltonians relevant to diatomic molecules are considered in this study. We consider that a molecule occupies the $v=0$ and $J=0$ ($N=0$) ground state before interaction with light. A femtosecond shaped MIR pulse (pump pulse) induces rovibrational transitions, and creates a rovibrational wave-packet in the electronic ground state. Figure 1 shows the one-photon allowed rovibrational transitions in the two different electronic states ($^1\Sigma$ and $^2\Pi$) for low J rotational states. In the $^1\Sigma$ state (X state of CO, N_2, and so on), only the P ($\Delta J=-1$) and R ($\Delta J=+1$) rovibrational transitions are allowed. Thus the lowest rovibrational state ($v=0$, $J=0$) can be coupled with the states of even v and even J or the states of odd v and odd J. On the other hand, the electron spin makes the coupling scheme complicated in the $^2\Pi$ state (X state of NO, OH, and so on). In this case, since all the P, Q ($\Delta J=0$), and R branches are allowed, all the rovibrational states can be coupled to each other.

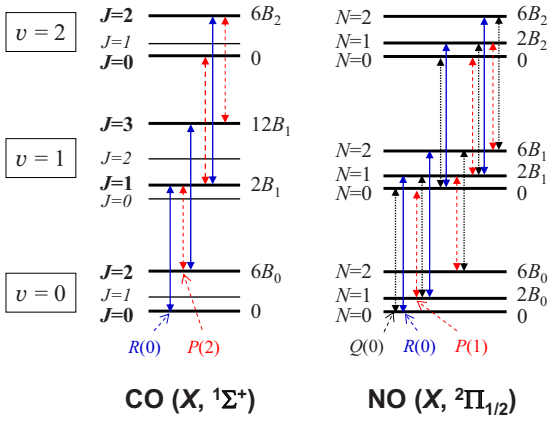

FIG. 1. (Color online) Schematic rovibrational energy diagram in the $X(^1\Sigma)$ state of CO and in the $X(^2\Pi)$ state of NO. The solid, dashed, and dotted arrows show the one-photon allowed transitions for R, Q, and P branches, respectively, in spectroscopic notation. The symbols shown in the right-hand side show the energy of rotational levels in each vibrational states. The symbols B_0, B_1, and B_2 correspond to the rotational constants in the $v=0$, 1, and 2 vibrational states, respectively.

A. Hamiltonian

In this study, linearly polarized light is employed to manipulate molecular wave-packets. The time dependence of molecular wave function $\Psi(t)$ is given by the Schrödinger equation as

$$i\hbar\frac{d\Psi(t)}{dt}=H(t)\Psi(t)=[H_0+H_1(t)+H_2(t)]\Psi(t). \quad (1)$$

H_0 is the zero-order molecular rovibrational Hamiltonian, and $H_1(t)$ and $H_2(t)$ represent the interaction between the molecule and the laser field *via* the dipole moment and polarizability, respectively. Since we consider the case where the femtosecond pulse contains a resonant frequency of vibrational transition, the term of the first-order dipole interaction is dominant compared with the polarizability term. If the

laser pulse does not contain a resonant frequency of molecules, contribution of the dipole interaction term is rapidly diminished due to time averaging. In such a case, the second-order interaction *via* polarizability becomes more important.

The dipole interaction term is described as

$$H_1(t) = -\vec{\mu}\cdot\vec{\varepsilon}(t) = -\mu\varepsilon(t)\cos\theta = -\mu\varepsilon(t)P_1(\cos\theta), \quad (2)$$

where μ is the dipole operator, $P_l(\cos\theta)$ are the Legendre polynomials of order l, θ is the polar angle between the molecular axis and the polarization of the electric field of linearly polarized light, and $\varepsilon(t)$ is a complex function of the electric field of laser pulse. The interaction *via* the polarizability is given by

$$H_2(t) = -\frac{1}{2}\vec{\varepsilon}(t)^*\boldsymbol{\alpha}\vec{\varepsilon}(t) = -\frac{1}{2}\varepsilon(t)^2\left[\alpha + \frac{2\gamma}{3}P_2(\cos^2\theta)\right]. \quad (3)$$

The isotropic polarizability, α, and the anisotropic polarizability, γ, are related to the diagonal elements of the polarizabilities with respect to the molecular fixed x', y', and z' components, $\alpha_{x'}=\alpha_{y'}=\alpha_\perp$ and $\alpha_{z'}=\alpha_\parallel$, as $\alpha=s(\alpha_{x'}+\alpha_{y'}+\alpha_{z'})/3$ and $\gamma=\alpha_{z'}-\alpha_{x'}$. The electric field $\varepsilon(t)$ is written as

$$\varepsilon(t) = \frac{f(t)}{2}\{\exp[-i(\varphi(t)+2\pi\nu_0 t)] + \text{c.c.}\}, \quad (4)$$

where $f(t)$ and $\varphi(t)$ are the amplitude and phase profiles of the electric field, respectively, and ν_0 is the center frequency of the laser pulse. The field amplitude profile $f(t)$ is related to the laser intensity profile $I(t)$ as

$$f(t) = \sqrt{\frac{2I(t)}{c\varepsilon_0}}, \quad (5)$$

where c is the speed of light and ε_0 is the permittivity of the vacuum.

B. Rovibrational wave-packets

1. $^1\Sigma$ states

First, we consider the rovibrational wave-packet in the $^1\Sigma$ electronic state. The time-dependent rovibrational state $|\Psi(t)\rangle$ can be expanded in terms of the rotational $|JM\rangle$ and vibrational $|v\rangle$ states as follows:

$$|\Psi(t)\rangle = \sum_v \sum_{JM} C_{v,JM}(t)|v\rangle|JM\rangle, \quad (6)$$

where v is the vibrational quantum number, J is the total angular momentum quantum number, and M is the projection quantum number of J along the space fixed axis. The states $|v\rangle|JM\rangle$ are eigenstates of the Hamiltonian H_0 in Eq. (1). The expansion coefficients $C_{v,JM}(t)$, which are complex variables, are obtained by substituting Eq. (6) into the time-dependent Schrödinger equation in Eq. (1), multiplying $\langle J'M'|\langle v'|$ from the left-hand side, and integrating over the space. With the help of the relation

$$\langle J'M'|P_l(\cos\theta)|JM\rangle = (-1)^{M'}[(2J+1)(2J'+1)]^{1/2} \times \begin{pmatrix} J & J' & l \\ M & -M' & 0 \end{pmatrix}\begin{pmatrix} J & J' & l \\ 0 & 0 & 0 \end{pmatrix}, \quad (7)$$

we obtained the differential equations for the coefficients $C_{v,JM}(t)$ as

$$\begin{aligned} i\hbar\frac{dC_{v,JM}(t)}{dt} = {} & E_{v,JM}C_{v,JM}(t) - \varepsilon(t)\sum_{J'=J\pm1}\sum_{v'} C_{v',J'M}(t) \\ & \times\langle v|\mu|v'\rangle(-1)^M[(2J+1)(2J'+1)]^{1/2} \\ & \times\begin{pmatrix} J & J' & 1 \\ M & -M & 0 \end{pmatrix}\begin{pmatrix} J & J' & 1 \\ 0 & 0 & 0 \end{pmatrix} \\ & - \frac{\varepsilon(t)^2}{2}\sum_{J'=J\pm2,J}\sum_{v'} C_{v',J'M}(t)\Bigg[\delta_{JJ'}\langle v|\alpha|v'\rangle \\ & + (-1)^M\frac{2}{3}\langle v|\gamma|v'\rangle[(2J+1)(2J'+1)]^{1/2} \\ & \times\begin{pmatrix} J & J' & 2 \\ M & -M & 0 \end{pmatrix}\begin{pmatrix} J & J' & 2 \\ 0 & 0 & 0 \end{pmatrix}\Bigg], \end{aligned} \quad (8a)$$

where $E_{v,JM}$ is the eigenenergy of the state $|v\rangle|JM\rangle$, and Wigner $3j$ symbols are used. In the following calculation, we treated femtosecond pulses that contain the transition frequency of $v=1\leftarrow v=0$. Therefore, it is reasonable to assume that

$$\sum_{v'} C_{v',JM}(t)\langle v|\mu|v'\rangle = C_{v+1,JM}(t)\langle v|\mu|v+1\rangle + C_{v-1,JM}(t) \times\langle v|\mu|v-1\rangle, \quad (8b)$$

$$\sum_{v'} C_{v',JM}(t)\langle v|\alpha|v'\rangle = C_{v,JM}(t)\langle v|\alpha|v\rangle, \quad (8c)$$

and

$$\sum_{v'} C_{v',JM}(t)\langle v|\gamma|v'\rangle = C_{v,JM}(t)\langle v|\gamma|v\rangle. \quad (8d)$$

In other words, we neglect off-resonant transitions of $\Delta v \geq 2$ for the dipole interaction and those of $\Delta v \geq 1$ for the interaction *via* the polarizability. If a pulse does not contain the resonant frequency, these off-resonant transitions become important. From $3j$ symbols in Eq. (8a), the selection rule of $\Delta J=\pm1$ and $\Delta M=0$ is derived for a process of the single dipole transition, while the selection rule of $\Delta J=\pm2$, 0 and $\Delta M=0$ is derived for the interaction via the polarizability. Since there is no interaction that connects $\Delta M\neq0$, we omit the subscript M in Eq. (8a) in the following discussion by setting $M=0$ all the time. This is valid when we prepare the $|v=0,J=0\rangle$ state as an initial state by using the supersonic expansion in the gas phase, the sample in the quantum solids or liquids, and so on.

2. $^2\Pi$ states

NO and OH are favorite molecules for studies on spectroscopy and dynamics since these molecules are simple examples of open shell diatomic molecules. The ground electronic state of both molecules is the $^2\Pi$ state which is split into two components $^2\Pi_{1/2}$ and $^2\Pi_{3/2}$ states by spin-orbit interaction. Since the spin-orbit coupling parameters are relatively large for both molecules (123 cm^{-1} for NO [62], and -139 cm^{-1} for OH [63]), the mixing between $^2\Pi_{1/2}$ and $^2\Pi_{3/2}$ states is negligible in low J states. The wave function $\Psi(t)$, therefore, can be expanded in terms of the Hund's case (a) basis functions as follows:

$$\Psi(t) = \sum_{v} \sum_{J\Omega M} C_{v,J\Omega M}(t)|v\rangle|J\Omega M\rangle, \tag{9}$$

where Ω is the projection of J along the molecular axis. In a similar way as in the case of $^1\Sigma$ states, the differential equations for the coefficients $C_{v,J\Omega M}(t)$ are obtained as follows:

$$\begin{aligned} i\hbar\frac{dC_{v,J\Omega M}(t)}{dt} &= E_{v,J\Omega M}C_{v,J\Omega M}(t) - \varepsilon(t)\sum_{J'=J\pm1,J}\sum_{v'} C_{v',J'\Omega M}(t)\langle v|\mu|v'\rangle[(2J+1)(2J'+1)]^{1/2}(-1)^{M-\Omega}\begin{pmatrix} J & J' & 1 \\ M & -M & 0 \end{pmatrix} \\ &\times\begin{pmatrix} J & J' & 1 \\ \Omega & -\Omega & 0 \end{pmatrix} - \frac{\varepsilon(t)^2}{2}\sum_{J'=J\pm2,J\pm1,J}\sum_{v'} C_{v',J'\Omega M}(t)\Bigg[\delta_{JJ'}\langle v|\alpha|v'\rangle + (-1)^{M-\Omega}\frac{2}{3}\langle v|\gamma|v'\rangle[(2J+1)(2J'+1)]^{1/2} \\ &\times\begin{pmatrix} J & J' & 2 \\ M & -M & 0 \end{pmatrix}\begin{pmatrix} J & J' & 2 \\ \Omega & -\Omega & 0 \end{pmatrix}\Bigg]. \end{aligned} \tag{10}$$

We also assumed Eqs. (8b)–(8d) for the dipole and polarizability matrices. From $3j$ symbols, the rotational selection rule is obtained as $\Delta J=\pm1, 0$ and $\Delta M=\Delta\Omega=0$ for the dipole interaction and $\Delta J=\pm2, \pm1, 0$ and $\Delta M=\Delta\Omega=0$ for the interaction *via* polarization.

III. RESULTS AND DISCUSSION

In this section, we apply the formalism summarized above to calculate the dynamics of rovibrational wave-packets on the X state of CO and NO created by femtosecond pulses. As laser pulses, we treat the simplest cases of a Fourier transform limited pulse with various intensities and pulse width, a linearly chirped pulse, and a double transform limited pulse.

The differential equations (8a) and (10) were solved by the fourth-order Runge-Kutta method with time steps of 0.1 fs which is much smaller than the oscillation period of the electric field of laser pulses (16.7 fs for the pulse with 5 μm wavelength). Throughout this study, we assumed that the molecules occupy only a single lowest energy state, that is, $|v=0,J=0\rangle$ for CO and $|v=0,\Omega=1/2,N=0\rangle$ for NO, as the initial rovibrational state, when N is the quantum number of the total angular momentum excluding electron spin. Maximum rotational and vibrational quantum numbers included in the calculations were $J_{\max}$ $(N_{\max})=10$ and $v_{\max}=6$. For CO in the $X(^1\Sigma^+)$ state, we used the molecular constants listed in Ref. [64] to calculate $E_{v,J}$ in Eq. (8a). The dipole matrix elements for vibrational transition $\langle v|\mu|v+1\rangle$ were taken from Ref. [65]. The polarizabilities were assumed to be $\langle v|\alpha|v\rangle=\alpha_0$ and $\langle v|\gamma|v\rangle=\gamma_0$ with $\alpha_0/4\pi\varepsilon_0=1.95$ Å^3 and $\gamma_0/4\pi\varepsilon_0=0.975$ Å^3 [66]. For NO in the $X(^2\Pi_{1/2})$ state, the molecular constants and the dipole matrix elements were taken from Refs. [67,68], respectively. The polarizabilities were $\alpha_0/4\pi\varepsilon_0=1.71$ Å^3 and $\gamma_0/4\pi\varepsilon_0=0.83$ Å^3 [69,70].

A. Wave-packet dynamics in the $^1\Sigma$ state

1. Transform-limited pulse

First, we discuss the wave-packet dynamics in the $X(^1\Sigma^+)$ state of CO created by a transform-limited pulse. The laser pulses employed in this calculation is defined in Eq. (4) with $f(t)=E_0\exp(-t^2/2\sigma_t^2)$. The center frequency of the laser pulse is fixed to the transition frequency of $|v=1,J=1\rangle \leftarrow |v=0,J=0\rangle$ which is $\nu_0=2147$ cm^{-1} [64]. Since the lowest energy state $|v=0,J=0\rangle$ which we assumed as the initial state can couple only with the $|v=1,J=1\rangle$ state *via* one-photon transition, the two-level system of $|v=0,J=0\rangle$ and $|v=1,J=1\rangle$ is a good candidate for a one-qubit system of quantum computation.

Figure 2(a) shows the electric field of the laser pulse we used in the calculation. The peak intensity of the laser pulse was set to $I_0=c\varepsilon_0E_0^2/2=0.81$ TW/cm^2 which corresponds to a pulse with the energy of 2.5 μJ focused down to 50 μm in diameter. The full width at the half maximum (FWHM) in the intensity was set to $\Delta t=2\sqrt{\ln 2}\sigma_t=147$ fs which corresponds to the frequency width (FWHM) of 100 cm^{-1}. Figure 2(b) shows the calculated time evolution of the coefficient $C_{v,J}(t)$ in the $X(^1\Sigma^+)$ of CO created by the pulse in Fig. 2(a). Note that Fig. 2(b) shows the amplitude of the wave function so that the population is obtained as the square, $|C_{v,J}(t)|^2$. Due to the selection rule of the $^1\Sigma$-$^1\Sigma$ transition, the accessible states from the lowest rovibrational state $|v=0,J=0\rangle$ are those of even v and even J or odd v and odd J. With this pulse, about 76% of the population remains in the initial state. The population transfer is mainly to the $|v=1,J=1\rangle$ state through the one-photon $R(0)$ transition which amounts to 18%. Higher rovibrational states such as $|v=2,J=0\rangle$, $|v=2,J=2\rangle$, and $|v=0,J=2\rangle$ are also excited by the pulse through multiphoton excitations, but the total population transfer to those higher states is only $\sim$4%.

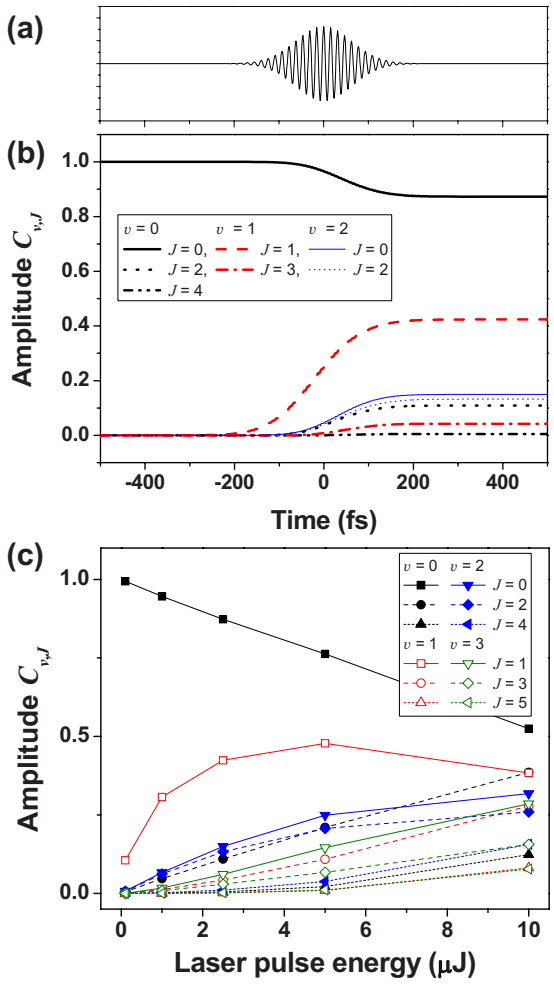

FIG. 2. (Color online) (a) Time profile of the transform-limited laser field amplitude $\mathrm{Re}(\varepsilon(t))$ with the FWHM of $\Delta t=147$ fs. The pulse energy and the focus diameter of 2.5 μJ and 50 μm, respectively, were used in the calculation. (b) Time evolution of the amplitude $C_{v,J}(t)$ of rovibrational states in the $X(^1\Sigma)$ of CO. The initial rovibrational state is $|v=0,J=0\rangle$. (c) Laser pulse energy dependence of the amplitude $C_{v,J}(t)$ at the end of population transfer. A laser pulse with $\Delta t=147$ fs focused down to 50 μm was employed.

Figure 2(c) presents the dependence of laser pulse energy on the amplitude $C_{v,J}(t)$ of rovibrational states at the end of population transfer. In this calculation, a laser pulse with $\Delta t=147$ fs focused down to 50 μm was employed with various laser pulse energies. The population in the $|v=0,J=0\rangle$ initial state monotonically decreases as the laser pulse energy increases. At the energy of 10 μJ, about 72% of population in the $|v=0,J=0\rangle$ state is transferred to the other states. By changing the pulse energy, we found that the population transfer to the $|v=1,J=1\rangle$ state becomes maximum ($\sim$23%) with a pulse energy of $\sim$5 μJ. Above this energy, multiphoton processes are induced and many rovibrational levels are occupied resulting in less population in the $|v=1,J=1\rangle$ state. There is an optimal laser power to suppress the population transfer to rovibrational states other than the target $|v=1,J=1\rangle$ state in the two-level system.

Figure 3 shows the dependence of pulse width on the time evolution of the amplitude $C_{v,J}(t)$. Transform-limited laser

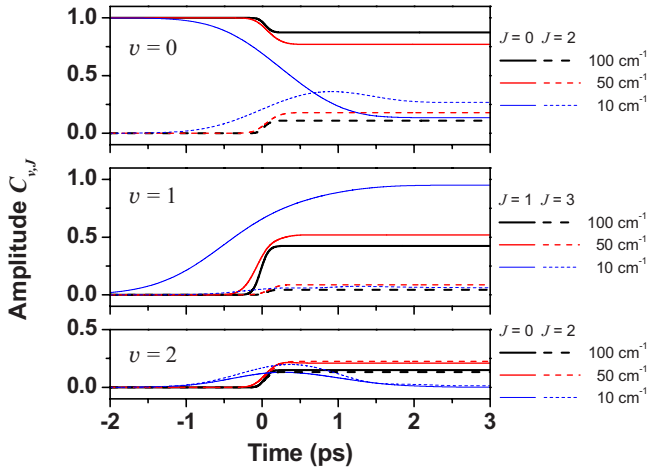

FIG. 3. (Color online) Dependence of laser pulse width on the time evolution of the amplitude $C_{v,J}(t)$ of rovibrational states in the $X(^1\Sigma)$ state of CO. A transform-limited laser pulse was assumed, and the calculated pulse width is listed in Table I. The thick, normal, and thin lines correspond to the spectral width of 100, 50, and 10 cm^{-1}, respectively. The pulse energy and the focus diameter in the calculation were 2.5 μJ and 50 μm, respectively. The initial rovibrational state is $|v=0,J=0\rangle$.

pulses with three different pulse widths listed in Table I were used. The pulse energy and the focus diameter in the calculation were 2.5 μJ and 50 μm, respectively, whose peak intensities are also listed in Table I.

As the pulse width is stretched from 150 fs to 1.5 ps, the population in the $|v=0,J=0\rangle$ state is decreased, and that of the $|v=1,J=1\rangle$ state is increased. With the pulse of $\Delta t=1.5$ ps time width and $\Delta\nu=10$ cm^{-1} frequency width in FWHM, only little population (2%) remains in the $|v=0,J=0\rangle$ state, and almost all the population is transferred to the $|v=1,J=1\rangle$ state (90%). In the view of quantum computation, if we consider the two-level system consisting of only $|v=0,J=0\rangle$ and $|v=1,J=1\rangle$ states, the ps pulse ($\Delta t=1.5$ ps, $\Delta\nu=10$ cm^{-1}) seems to be appropriate for the NOT quantum gate operation. However, in the actual molecules, the other rovibrational states such as $|v=0,J=2\rangle$ and $|v=1,J=3\rangle$ are also populated after interaction with the laser pulse. The total population in other states is about 8%, which is still small but could cause significant errors in the quantum computation. The longer pulse mainly induces the downward transition of $|v=1,J=1\rangle\rightarrow|v=0,J=2\rangle$ during the pulse excitation, since the narrower band laser ($\Delta\nu=10$ cm^{-1}) does not contain a frequency component corresponding to the vibrational

TABLE I. Calculated pulse width and peak intensity of the laser pulses used in the calculation shown in Fig. 3. Transform-limited pulse with the energy of 2.5 μJ is assumed.

Spectral width $\Delta\nu$ (cm^{-1})	Pulse width Δt (fs)	Peak intensity I_0 (TW/cm^2)
100	147	0.81
50	294	0.41
10	1471	0.08

transition of $v=2\leftarrow v=1$ whose transition frequency is 2120 cm^{-1}. The energy difference between the $v=1\leftrightarrow v=0$ and $v=2\leftrightarrow v=1$ transition is 27 cm^{-1}, which is caused by the anharmonicity. On the other hand, shorter pulses induce the upward transition of $|v=2,J=0\rangle$ or $|v=2,J=2\rangle\leftarrow|v=1,J=1\rangle$ more efficiently. This is because the transition of $v=2\leftarrow v=1$ can be excited by the broadband laser pulse ($\Delta\nu=100$ cm^{-1}) resonantly. In addition, the transition dipole moment $\langle 2|\mu|1\rangle$ is larger than that in $\langle 1|\mu|0\rangle$ [65], which also accelerates the $v=2\leftarrow v=1$ excitation. The results shown in Fig. 3 seem to suggest that the longer duration pulse is appropriate for maximizing population transfer. However, the short pulse with broad spectral width is essentially required to excite several vibrational modes to construct multiqubit systems [49]. To suppress the unwanted transitions for the quantum computation such as $|v=1,J=1\rangle\rightarrow|v=0,J=2\rangle$ in quantum gate operations, it is necessary to shape laser pulses. In the next two sections, we examine the effect of the

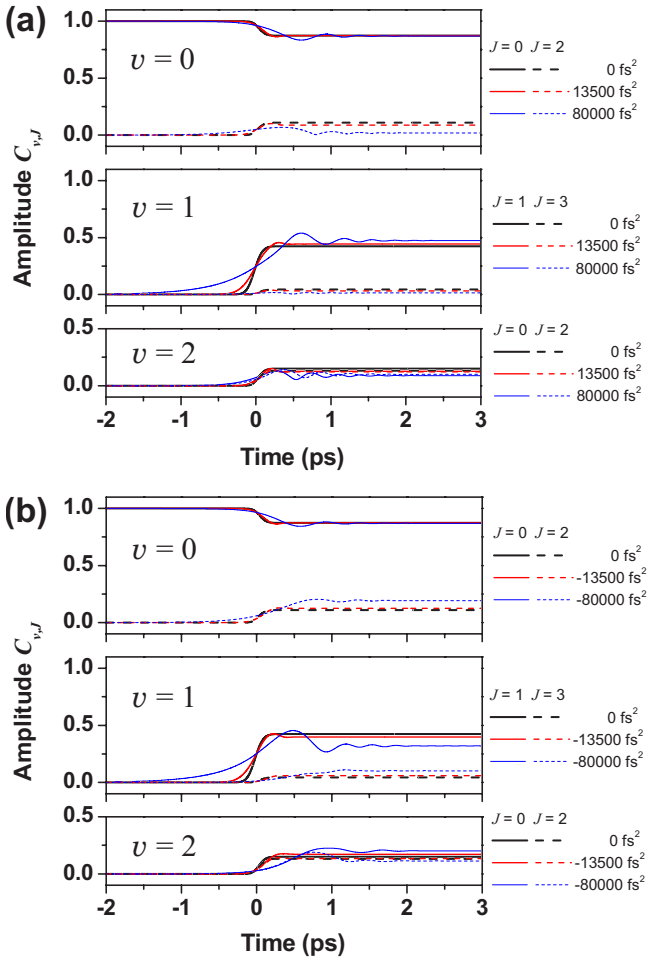

FIG. 4. (Color online) Chirp dependence of the time evolution of the amplitude $C_{v,J}(t)$ in rovibrational states in the $X(^1\Sigma)$ of CO for the (a) positive ($x>0$) and (b) negative ($x<0$) chirps. The thick, normal, and thin lines correspond to the chirp of $x=0$, $\pm 13\,500$, and $\pm 80\,000$ fs^2, respectively. The spectral width, the pulse energy, and the focus diameter in the calculation were 100 cm^{-1}, 2.5 μJ, and 50 μm, respectively. The calculated pulse width is listed in Table II. The initial rovibrational state is $|v=0,J=0\rangle$.

TABLE II. Pulse width and peak intensity of chirped laser pulses used in the calculation shown in Fig. 4. The spectral width of 100 cm^{-1} and the energy of 2.5 μJ are assumed.

Chirp x (fs^2)	Pulse width Δt (fs)	Peak intensity I_0 (TW/cm^2)
0	147	0.81
$\pm 13\,500$	294	0.41
$\pm 80\,000$	1514	0.08

chirp and double pulses as the simplest shaped pulses, and compare the results with those obtained by the transform-limited pulse.

2. Linearly chirped pulses

The electric field $\varepsilon(t)$ in Eq. (4) used in the calculation for linearly chirped pulses is the Fourier transform of the following electric field in the frequency domain,

$$E(\omega)\propto\exp\left\{-\frac{(\omega-\omega_0)^2}{2\sigma_\omega^2}\right\}\exp\left\{\frac{ix(\omega-\omega_0)^2}{2}\right\}, \quad (11)$$

where x is the linear chirp, $\omega=2\pi\nu$ is the angular frequency of the pulse, and $\sigma_\omega=\Delta\omega/(2\sqrt{\ln 2})$ corresponds to the spectral width of the pulse which was fixed to $\Delta\nu=\Delta\omega/2\pi=3$ THz (100 cm^{-1}). Figure 4 shows the chirp dependence on the time evolution of the amplitudes $C_{v,J}(t)$ in the $X(^1\Sigma)$ electronic state of CO. The pulse width Δt and the peak intensity of each chirp pulse are listed in Table II. The chirps chosen in the calculation were such that the temporal pulse width stretched by each chirp is close to that of each transform-limited pulse listed in Table I. The pulse energy and the focus diameter were assumed to be 2.5 μJ and 50 μm, respectively. As seen in Fig. 4, the chirp dependence on the time evolution of the wave-packet is not drastic as compared with the dependence of spectral width by the transform-limited pulses shown in Fig. 3. In the transform-limited pulses, the spectral density at the resonance frequency increases as the laser pulse width increases in time. As a result, the population transfer from $|v=0,J=0\rangle$ to $|v=1,J=1\rangle$ is enhanced with longer laser pulse. On the other hand, since the spectral density does not depend on chirp, the population transfer is not enhanced drastically by increasing the temporal width.

In the case of negatively chirped pulses of $x=-80\,000$ fs^2, the population in the $|v=1,J=1\rangle$ state is reduced compared with other pulses, and the successive transitions to $|v=0,J=2\rangle$, $|v=2,J=0\rangle$, $|v=2,J=2\rangle$, etc. are induced. On the contrary, the successive transitions are suppressed in the case of positively chirped pulses. It is seen that the negatively chirped pulses enhance the ladder climbing [33,35–39].

3. Double pulses in time domain

The field amplitude we used in the calculation is

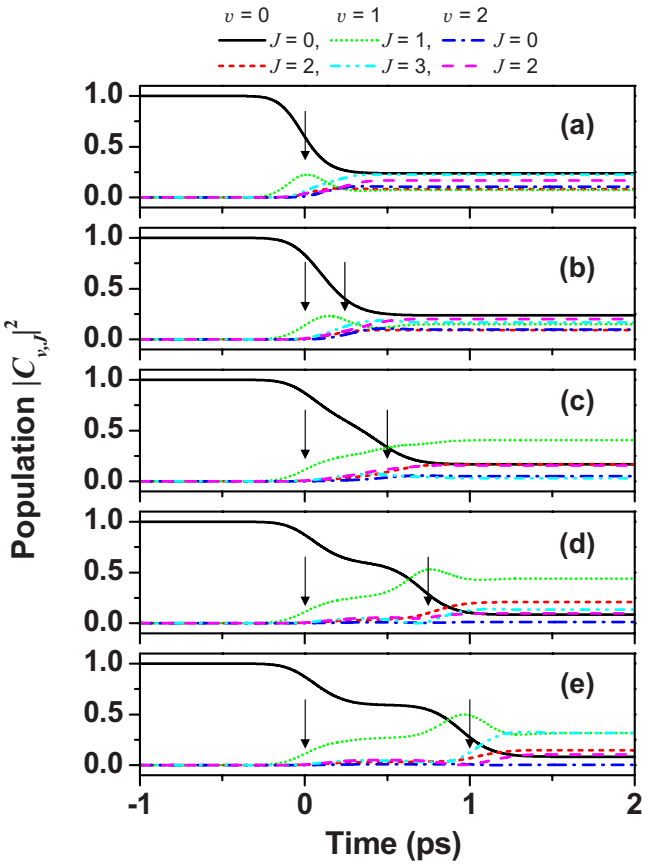

FIG. 5. (Color online) Time evolution of the rovibrational state population, $|C_{v,J}|^2$, in the $X(^1\Sigma)$ of CO when the double pulse with the relative phase of $\phi=0$ is applied. The initial rovibrational state is $|v=0,J=0\rangle$. The transform-limited laser pulse ($\Delta t=294$ fs and $\Delta\nu=50$ cm^{-1}) was assumed for each pulse in the pulse pairs. The pulse energy and the focus diameter in the calculation were 2.5 μJ and 50 μm, respectively. The time separations t_0 of the pulse pairs were (a) 0 ps, (b) 0.25 ps, (c) 0.5 ps, (d) 0.75 ps, and (e) 1 ps. The arrows show the peaks of the laser pulses.

$$f(t) = E_0\left[\exp\left\{-\frac{(t-t_0/2)^2}{2\sigma_t^2}\right\} + \exp\left\{-\frac{(t+t_0/2)^2}{2\sigma_t^2}\right\} \times \exp(-i\phi)\right], \quad (12)$$

where t_0 is the time separation between two pulses and ϕ is the relative phase between the pulse pair. We only consider the case where there is no linear chirp. The transform-limited laser pulse [$\Delta t=294$ fs and $\Delta\nu=1.5$ THz (50 cm^{-1})] with $I_0=0.41$ TW/cm^2 corresponding to a 2.5 μJ pulse focused to 50 μm is assumed for each pulse in the pulse pairs. Figure 5 shows time evolution of the rovibrational state population, $|C_{v,J}|^2$ (not the amplitude $C_{v,J}$), in the $X(^1\Sigma)$ state of CO caused by the interaction with the double pulses. The relative phase ϕ of the pulse pair was set to zero in the calculation. When the pulse pair is completely overlapped [Fig. 5(a)], the population transfer from the initial state is about 76%. As the time separation increases to 750 fs, the ratio of the transfer increases up to 92%. When the separation is longer than

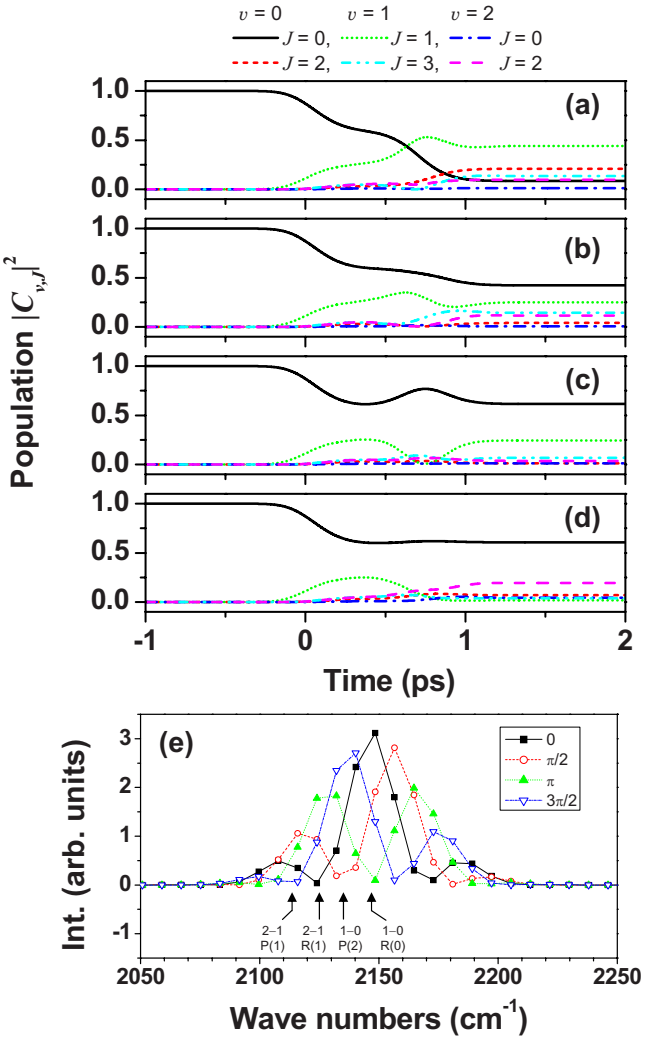

FIG. 6. (Color online) Time evolution of the rovibrational state population, $|C_{v,J}|^2$, in the $X(^1\Sigma)$ of CO when the double pulse interacts. The initial rovibrational state is $|v=0,J=0\rangle$. The transform-limited laser pulse ($\Delta t=294$ fs and $\Delta\nu=50$ cm^{-1}) was assumed for each pulse in the pulse pairs, but the relative phases ϕ of the front pulse with respect to the delayed pulse were (a) 0, (b) $\pi/2$, (c) π, and (d) $3\pi/2$. The pulse energy and the focus diameter in the calculation were 2.5 μJ and 50 μm, respectively. The time separation of the pulse pairs was 0.75 ps. (e) Spectra of the pulse pairs caused by the interference between two pulses. The arrows indicate the transition frequencies involved in this study.

750 fs, no further enhancement of the population transfer is observed. After the interaction, the population in the $|v=1,J=1\rangle$ state increases from 7% for $t_0=0$ fs to 44% for $t_0=750$ fs. The population in the $|v=1,J=1\rangle$ state does not increase with pulses longer than 750 fs, but decreases above 1 ps.

Double pulses in time domain have often been employed to realize coherent control in chemical reaction and quantum computation [54]. In the view of the quantum computation, the fidelity of the $|v=1,J=1\rangle \leftarrow |v=0,J=0\rangle$ transition as a NOT gate is not satisfactory, since the population in the $|v=1,J=1\rangle$ state is only 44%. In the case of the pulses of $t_0=750$ fs, the $|v=1,J=1\rangle \rightarrow |v=0,J=2\rangle$ transition is induced

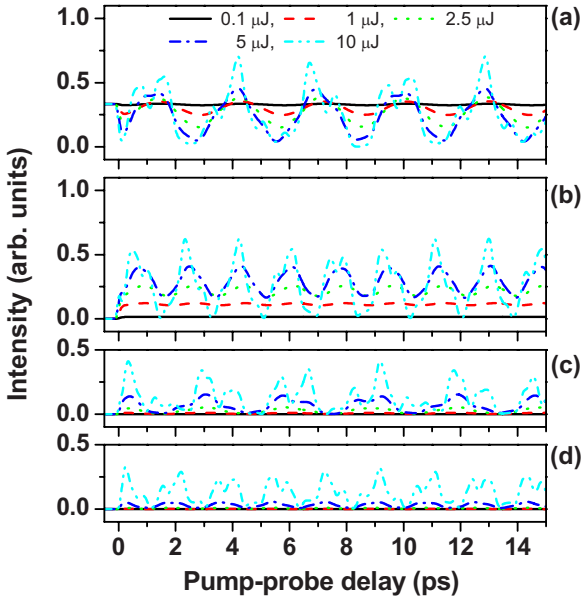

FIG. 7. (Color online) Pump pulse energy dependence of the time profile of the transition intensities from the (a) $v_g=0$, (b) $v_g=1$, (c) $v_g=2$, and (d) $v_g=3$ vibrational states in the $X(^1\Sigma)$ state to $B(^1\Sigma)$ electronic state of CO. The laser focus diameter in calculation was 50 μm. The transform-limited laser pulse ($\Delta t=147$ fs and $\Delta\nu=100$ cm^{-1}) was assumed.

by the second pulse, which disturbs the realization of the NOT gate. This is an inherent difficulty in controlling the wave-packet dynamics in molecular systems with rotational states.

Figure 6 shows the effect of the relative phase in the double pulse experiments. The time separation of the pulse pairs was fixed to 750 fs in the calculation. As seen in Fig. 6, the population transfer significantly depends on the relative phase. When the relative phase of the front pulse is $\pi/2$ with respect to the delayed pulse, the resultant population shown in Fig. 6(b) indicates that a Hadamard gate is almost realized

$$|v=0,J=0\rangle \rightarrow \frac{1}{\sqrt{2}}(|v=0,J=0\rangle + |v=1,J=1\rangle). \quad (13)$$

The populations of the $|v=0,J=0\rangle$ and $|v=1,J=1\rangle$ states after the interaction with the pulse pair were 42% and 25%, respectively. As the relative phase increases to π, the delayed pulse induces a backward transition of $|v=1,J=1\rangle \rightarrow |v=0,J=0\rangle$ resulting in the population in $|v=0,J=0\rangle$ to 62%. Although this behavior is different from the result obtained by Troppmann and Vivie-Riedle using the normal modes of acetylene [54], where the pulse with a relative phase of $\pi/2$ realizes the Hadamard gate, we can qualitatively explain our result by the spectra of the interfering pulse pairs. The interference spectral structures due to the double pulses are shown in Fig. 6(e), which depends on the relative phase of the pulse pairs. At the zero relative phase, the pulse intensity at the frequency corresponding to the $|v=1,J=1\rangle \leftarrow |v=0,J=0\rangle$ transition, $1-0$ $R(0)$ in Fig. 6(e), is the most intense, and therefore, the population transfer from the initial state occurs effectively. The successive transition of $|v=1,J=1\rangle \rightarrow |v=0,J=2\rangle$, however, is also induced, since the frequency component of this successive transition, $1-0$ $P(2)$, is also significant in the spectrum. When the relative phase of $\pi/2$ is applied, the spectrum is blueshifted. The population transfer from the initial state is suppressed as shown in Fig. 6(b) because of the decrease of the intensity corresponding to the $|v=1,J=1\rangle \leftarrow |v=0,J=0\rangle$ transition. On the other hand, since the intensity is almost zero at the frequency of the $|v=1,J=1\rangle \rightarrow |v=0,J=2\rangle$ transition in the spectrum of the pulse with $\phi=\pi/2$, the downward transition is not induced. Therefore, the population in the $|v=1,J=1\rangle$ remains after the pulse excitation. The small amount of population, however, transfers to the rovibrational states in $v=2$ due to the frequency component at the transitions of $|v=2,J=2\rangle \leftarrow |v=1,J=1\rangle$ and $|v=2,J=0\rangle \leftarrow |v=1,J=1\rangle$, which disturbs realization of the Hadamard gate in Eq. (13). With the relative phase of π, the frequency component of the transition $|v=1,J=1\rangle \leftarrow |v=0,J=0\rangle$ is almost null in the spectrum and the Hadamard gate cannot be realized.

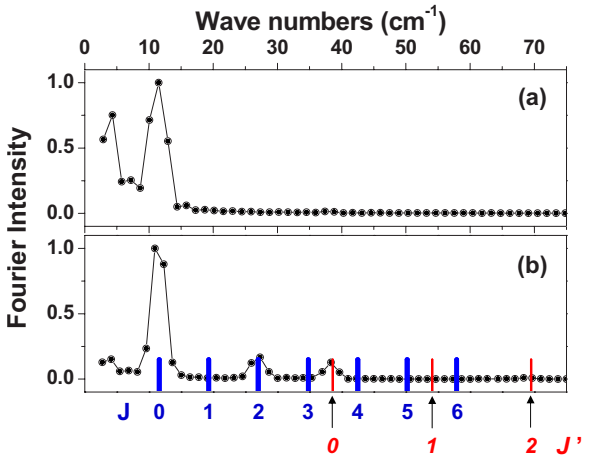

FIG. 8. (Color online) Fourier transforms of the time profiles of the transition intensities from the $X(v_g=0)$ vibronic state shown in Fig. 7(a). The laser pulse energies employed in calculation were (a) 2.5 μJ and (a) 10 μJ. The thick and thin bold sticks show the predicted beat frequencies by $\Delta\nu_{J+2,J}=2B(2J+3)$ and $\Delta\nu_{J'+4,J'}=4B(2J'+5)$, respectively.

B. Detection of wave-packet propagation

Experimentally, one can probe the rovibrational wave-packet propagation by applying additional pulse(s) to the system. Vibronic excitation by a broadband femtosecond UV pulse is an example of such probes. The transition intensity as a function of the delay time t between the first MIR pulse and the successive prove pulse contains information on the time evolution of the phase and amplitude of the rovibrational wave-packet created by the first MIR pulse. Even with a broadband femtosecond probe pulse, one can excite one of the vibrational states in the wave-packet selectively in the case of simple diatomic molecules. On the other hand, since the spectral bandwidth of a broadband femtosecond pulse is typically $\sim$100 cm^{-1}, most of the rotational states in a single vibrational state are excited coherently, and projected onto the excited electronic state. As a result, the coherence of the

rotational states in the wave-packet is detected as a modulation in the transition intensity as shown in the case of rotational coherence spectroscopy [71,72]. In this section, we examine the time profile of such a probe transition intensity when we create a rovibrational wave-packet in the ground electronic state of CO as discussed in the previous section. As a probe, we chose the $B(^1\Sigma) \leftarrow X(^1\Sigma)$ single-photon transition of CO at 115 nm, which has a strong transition moment.

After the pump pulse, the wave-packet propagates under the zero order Hamiltonian H_0 in Eq. (1). When the wave-packet is probed at a delay time t after the pump pulse through $B(^1\Sigma^+)$, $v=v_f \leftarrow X(^1\Sigma^+)$, $v=v_g$ transition, the state created in the excited $^1\Sigma$ vibronic state is written as

$$|\Psi^{\mathrm{ex}}(t)\rangle = \sum_{J_g M_g} C_{v_g,J_g M_g}(t) \sum_{J_f M_f} \langle J_f M_f|\vec{\mu}\cdot\vec{\varepsilon}|J_g M_g\rangle |v_f\rangle |J_f M_f\rangle, \tag{14}$$

where the subscripts g and f indicate the parameters in the ground and excited electronic states, respectively. The rotational transition matrix element $\langle J_f M_f|\vec{\mu}\cdot\vec{\varepsilon}|J_g M_g\rangle$ is proportional to $\langle J_f M_f|P_1(\cos\theta)|J_g M_g\rangle$ defined in Eq. (7), when linearly polarized probe light is employed. Then, the transition intensity is obtained as follows:

$$\begin{aligned} I(t) = \langle \Psi^{\mathrm{ex}}(t)|\Psi^{\mathrm{ex}}(t)\rangle &\propto \sum_{M_g} \sum_{J_{g'} J_{g''}} C_{v_g,J_{g'}M_g}(t) C_{v_g,J_{g''}M_g}(t)^* \sum_{J_{f'}J_{f''}} \langle J_{f'}M_g|\vec{\mu}\cdot\vec{\varepsilon}|J_{g'}M_g\rangle \langle J_{f''}M_g|\vec{\mu}\cdot\vec{\varepsilon}|J_{g''}M_g\rangle \\ &\times \int d\Omega\, Y_{J_{f'}M_g}(\theta,\phi) Y^*_{J_{f''}M_g}(\theta,\phi) \\ &\propto \sum_{M_g} \sum_{J_{g'}J_{g''}} [(2J_{g'}+1)(2J_{g''}+1)]^{1/2} C_{v_g,J_{g'}M_g}(t) C_{v_g,J_{g''}M_g}(t)^* \sum_{J_f} (2J_f+1) \\ &\times \begin{pmatrix} J_f & J_{g'} & 1 \\ M_g & -M_g & 0 \end{pmatrix} \begin{pmatrix} J_f & J_{g''} & 1 \\ M_g & -M_g & 0 \end{pmatrix} \begin{pmatrix} J_f & J_{g'} & 1 \\ 0 & 0 & 0 \end{pmatrix} \begin{pmatrix} J_f & J_{g''} & 1 \\ 0 & 0 & 0 \end{pmatrix}, \end{aligned} \tag{15}$$

where $Y_{JM}(\theta,\phi)=|JM\rangle$ is the spherical harmonics of order J.

Figure 7 shows the pump pulse energy dependence on the calculated transition intensity to the $B(^1\Sigma)$ electronic state from individual vibrational states of $v_g=0$, 1, 2, and 3 in the $X(^1\Sigma)$ state in the rovibrational wave-packet created by a simple transform-limited pulse shown in Fig. 2. We assume that the Frank-Condon factor $\langle v_f|v_g\rangle$ is equal to unity. Periodic revival structures can be seen in all of the time profiles of the transition intensity. When the low pump pulse energy is employed, the structure of the time profile of the detection intensity is a simple sinusoidal function. In contrast, at high pulse energies, the profiles that contain an interference pattern with a long period of ~9 ps are rather complicated, since many rotational states are involved in interference. The periodic structure originates in the interference of the rotational states in the ground electronic state coherently excited by a broadband femtosecond MIR laser pulse. The revival time is proportional to the inverse of the energy separation between the rotational states that are excited coherently by the pump pulse [71,72].

The long period is roughly $\tau_E=1/(2B_{v_g})$, where B_{v_g} is the rotational constant in each vibrational state of CO in units of Hz [71,72]. The estimated revival times are 8.63 ps, 8.71 ps, 8.79 ps, and 8.87 ps for the $v_g=0$, 1, 2, and 3 states, respectively, which are close to the revival times seen in Fig. 7.

Figure 8 shows the Fourier transforms of the time profiles of the transition intensities from the $X(v_g=0)$ vibronic state shown in Fig. 7(a). The Fourier transform of the time-dependent intensity profiles gives us information on the rotational state distribution of the rotational wave-packet in each vibrational state. The transformed spectrum shows a peak at the beat frequencies $\Delta\nu$ between the coupled rotational states, whose amplitude is proportional to the product of the coefficients of the coupled rotational states, $|C_{v_g,J_g'}||C_{v_g,J_g''}|$. Neglecting higher order rotational constants, the dominant beat frequencies are obtained as

$$\Delta\nu_{J+2,J} = B(J+2)(J+3) - BJ(J+1) = 2B(2J+3), \tag{16a}$$

for $\Delta J=2$, and

$$\Delta\nu_{J+4,J} = B(J+4)(J+5) - BJ(J+1) = 4B(2J+5), \tag{16b}$$

for $\Delta J=4$. As seen in Fig. 8(a), the single beat frequency $\Delta\nu_{2,0}$ only appeared at low pump energy of 2.5 μJ, since only the $J_g=0$ and 2 states are populated in the $v_g=0$ state. On the other hand, at high pulse energy of 10 μJ, the beat frequencies corresponding to the rotational state $J_g=4$ also appeared in the spectrum as shown in Fig. 8(b). Figure 8 tells us that the amplitude of rotational states in the rovibrational wave-packet can be obtained from the Fourier transform of the time profile of the transition intensity.

The effect of the phase difference in the excitation with double pulses clearly appears in the time profiles of the detection intensity of the rovibrational wave-packet. Figure 9 shows the calculated time profile of the transition intensities from the (a) $v_g=0$, (b) $v_g=1$, and (c) $v_g=2$ vibrational states

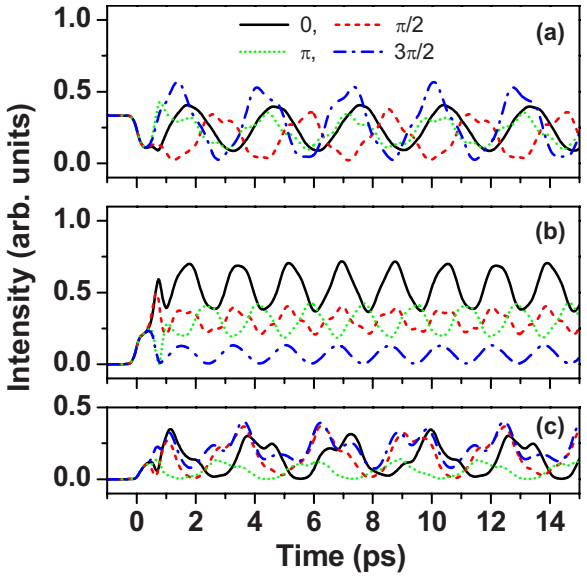

FIG. 9. (Color online) Time profiles of the transition intensities from the (a) $v_g=0$, (b) $v_g=1$, and (c) $v_g=2$ vibrational states in the $X(^1\Sigma)$ state to the $B(^1\Sigma)$ state of CO when a double pulse is applied. The transform-limited laser pulse ($\Delta t=294$ fs and $\Delta\nu=50$ cm^{-1}) was assumed for each pulse in the pulse pair with the relative phases of the front pulse with respect to the delayed pulse being 0 (solid line), $\pi/2$ (dashed line), π (dotted line), and $3\pi/2$ (dash-dotted line). The time separation of the pulse pairs was 0.75 ps. The peak intensity was $I_0=0.41$ TW/cm^2 of each pulse in the pulse pair.

in the $X(^1\Sigma)$ state to the $B(^1\Sigma)$ electronic state of CO when a double pulse with the time separation of 750 fs was used. The transform-limited laser pulse [$\Delta t=294$ fs and $\Delta\nu=1.5$ THz (50 cm^{-1})] was assumed for each pulse in the pulse pairs, and the relative phases of the front pulse with respect to the delayed pulse were set to be 0 (solid line), $\pi/2$ (dashed line), π (dotted line), and $3\pi/2$ (dash-dotted line). The phase of the modulation in the intensity profile shifts as the relative phase of the pulse pair is changed. This result indicates that the phase of the rovibrational states in the wave-packet can be finely manipulated by the relative phase of a pulse pair, and detected by the present detection scheme. Together with the Fourier transform analysis, one can determine the phase and relative amplitude of the rotational states in a wave-packet experimentally.

C. Wave-packet manipulation in the $^2\Pi$ state

In this section, the rovibrational wave-packet of NO molecule is discussed as an example of molecules in the doublet electronic state. As seen below, the different electronic states give completely different wave-packet behavior.

Figure 10 represents the time evolution of the rovibrational state population, $|C_{v,N}|^2$, in the $X(^2\Pi_{1/2})$ state of NO arising from the interaction with a double pulse. The initial rovibrational state was assumed to be $|v=0,\Omega=1/2,N=0\rangle$. The transform-limited laser pulse [$\Delta t=294$ fs and $\Delta\nu=1.5$ THz (50 cm^{-1})] was assumed for each pulse in the pulse pairs, with the relative phase of the front pulse with respect to the delayed pulse being (a) 0 and (b) π. The time

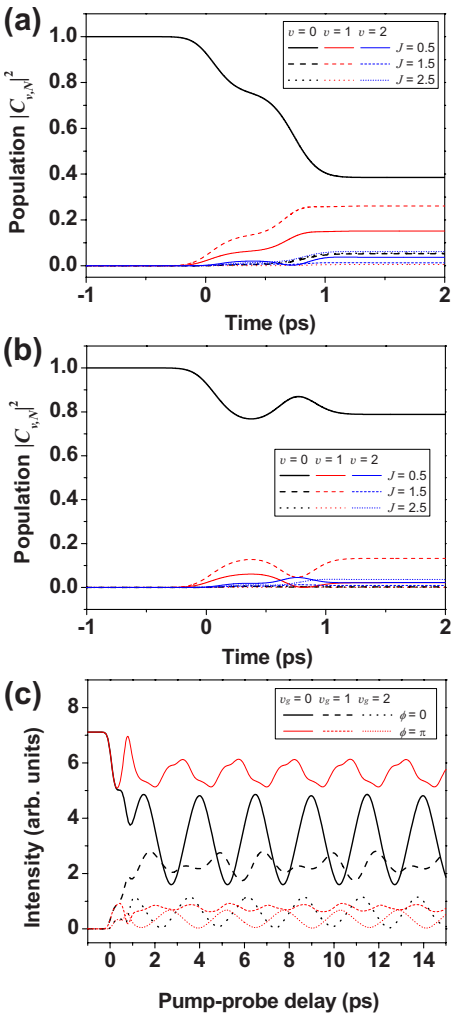

FIG. 10. (Color online) Time evolution of the rovibrational state population, $|C_{v,N}|^2$, in the $X(^2\Pi)$ of NO when a double pulse was applied. The initial rovibrational state is $|v=0,\Omega=1/2,N=0\rangle$. The transform-limited laser pulse ($\Delta t=294$ fs and $\Delta\nu=50$ cm^{-1}) was assumed for each pulse in the pulse pairs with the relative phase of the front pulse with respect to the delayed pulse being (a) 0 and (b) π. The time separation of the pulse pairs was 0.75 ps. The peak intensity of each pulse in the pulse pair was $I_0=0.41$ TW/cm^2. (c) Time evolution of the time profile of the transition intensities from the $v_g=0$, 1, and 2 vibrational states in the $X(^2\Pi)$ electronic state to the $A(^2\Pi)$ excited state of NO. The relative phases of the front pulse with respect to the delayed pulse were 0 (thick line) and π (thin line).

separation of the pulse pairs was 750 fs in the calculation shown in Fig. 10. The center frequency of the laser pulse was fixed to 1875 cm^{-1}, which is the middle of the frequencies between the $|v=1,N=1\rangle\leftarrow|v=0,N=0\rangle$ and $|v=1,N=0\rangle\leftarrow|v=0,N=0\rangle$ transitions. The pulse intensity was set to 0.41 TW/cm^2, which corresponds to the pulse energy of 2.5 μJ focused to the spot with 50 μm in diameter. Due to the selection rule of the $^2\Pi$-$^2\Pi$ transition, the lowest rovibrational state $|v=0,\Omega=1/2,N=0\rangle$ can be coupled with the states with $\Delta v=\pm1$ and $\Delta N=\pm1,0$. After the interaction with the pulse pair, the ratio of the population transfer from the initial state is about 61% and 21% for the relative phases

of 0 and π, respectively. The reason for the smaller population transfer for the relative phase of π than that for the phase of 0 is the same as in the case of CO. Since Q branch transitions are also allowed in the $^2\Pi$-$^2\Pi$ transition, the population is split into two states *via* the $Q(0)$ and $R(0)$ transitions. Due to the optical selection rule of $\Delta N = \pm 1$ and 0, doublet molecules are more difficult than singlet molecules to use as a two-level system for quantum computing.

Figure 10(c) shows the calculated transition intensity to the $A(^2\Sigma)$ excited state from individual vibrational states of the $X(^2\Pi_{1/2})$ ground state of NO. The periodic revival structure can be seen in all of the time profiles of the transition intensity. The revival time in each vibrational state is almost equal to $1/(2B_{v_g})$ as in the case of CO. The effect of the phase difference can be seen in the detection intensity profiles. The ratio of the population transfer in the doublet NO molecule is much smaller than that in the singlet CO molecule, since the vibrational transition moments of NO are smaller than those of CO.

IV. CONCLUSION

In this paper, we have examined rovibrational wave-packet dynamics in the ground electronic states manipulated by a shaped MIR femtosecond laser pulse. We have included the rotational states in our formalism explicitly. Since the rotational excitation selection rule is $\Delta J = \pm 1$ and $\Delta N = \pm 1$, 0 for the singlet $^1\Sigma$ and doublet $^2\Pi$ electronic states, respectively, multiple excitation pathways are formed to make the rovibrational wave-packet dynamics complicated. We have shown that one can suppress or enhance specific population transfer by applying chirped pulse and/or double pulses. But such simple pulses employed in the present work are not enough to realize the population transfer with high fidelity. For the application of molecules, therefore, to practice purposes such as quantum computation, optimization methods must be employed to find the best shape of pulses. Wave-packet dynamics manipulated by more complicated pulses will be discussed in a separate paper [61]. We have also demonstrated that the information on the phase and amplitude of the rovibrational wave-packet can be obtained by ionization or laser induced fluorescence signals. Establishment of such a detection system is also indispensable for the application of molecules to coherent control and quantum computation. The present results indicate that broadband excitation is useful for the detection of wave-packet dynamics. Experimental realization of such detection is now underway.

ACKNOWLEDGMENTS

This research was supported by Japan Science and Technology Agency under the CREST project, "Quantum Information Processing," and an NSERC Discovery Grant.

[1] M. Dantus and V. V. Lozovoy, Chem. Rev. (Washington, D.C.) **104**, 1813 (2004), and references therein.
[2] R. E. Carley, E. Heesel, and H. H. Fielding, Chem. Soc. Rev. **34**, 949 (2005), and references therein.
[3] V. V. Lozovoy and M. Dantus, ChemPhysChem **6**, 1970 (2005), and references therein.
[4] N. F. Scherer, A. J. Ruggiero, M. Du, and G. R. Fleming, J. Chem. Phys. **93**, 856 (1990).
[5] N. F. Scherer, R. J. Carlson, A. Matro, M. Du, A. J. Ruggiero, V. Romerorochin, J. A. Cina, G. R. Fleming, and S. A. Rice, J. Chem. Phys. **95**, 1487 (1991).
[6] N. F. Scherer, A. Matro, L. D. Ziegler, M. Du, R. J. Carlson, J. A. Cina, and G. R. Fleming, J. Chem. Phys. **96**, 4180 (1992).
[7] L. C. Zhu, V. Kleiman, X. N. Li, S. P. Lu, K. Trentelman, and R. J. Gordon, Science **270**, 77 (1995).
[8] O. Kinrot, I. S. Averbukh, and Y. Prior, Phys. Rev. Lett. **75**, 3822 (1995).
[9] C. Leichtle, W. P. Schleich, I. S. Averbukh, and M. Shapiro, J. Chem. Phys. **108**, 6057 (1998).
[10] V. Blanchet, M. A. Bouchène, and B. Girard, J. Chem. Phys. **108**, 4862 (1998).
[11] V. Szöcs, A. Tortschanoff, T. Pálszegi, C. Warmuth, and H. F. Kauffmann, J. Chem. Phys. **112**, 4652 (2000).
[12] C. Warmuth, A. Tortschanoff, F. Milota, M. Shapiro, Y. Prior, I. S. Averbukh, W. Schleich, W. Jakubetz, and H. F. Kauffmann, J. Chem. Phys. **112**, 5060 (2000).
[13] C. Warmuth, A. Tortschanoff, F. Milota, M. Leibscher, M. Shapiro, Y. Prior, I. S. Averbukh, W. Schleich, W. Jakubetz, and H. F. Kauffmann, J. Chem. Phys. **114**, 9901 (2001).
[14] R. Uberna, Z. Amitay, C. X. W. Qian, and S. R. Leone, J. Chem. Phys. **114**, 10311 (2001).
[15] K. Ohmori, H. Katsuki, H. Chiba, M. Honda, Y. Hagihara, K. Fujiwara, Y. Sato, and K. Ueda, Phys. Rev. Lett. **96**, 093002 (2006).
[16] H. Katsuki, H. Chiba, B. Girard, C. Meier, and K. Ohmori, Science **311**, 1589 (2006).
[17] W. S. Warren, J. Chem. Phys. **81**, 5437 (1984).
[18] D. J. Tannor and S. A. Rice, J. Chem. Phys. **83**, 5013 (1985).
[19] D. J. Tannor, R. Kosloff, and S. A. Rice, J. Chem. Phys. **85**, 5805 (1986).
[20] P. Brumer and M. Shapiro, Acc. Chem. Res. **22**, 407 (1989).
[21] U. Gaubatz, P. Rudecki, S. Schiemann, and K. Bergmann, J. Chem. Phys. **92**, 5363 (1990).
[22] S. Chelkowski, A. D. Bandrauk, and P. B. Corkum, Phys. Rev. Lett. **65**, 2355 (1990).
[23] N. V. Vitanov, K. A. Suominen, and B. W. Shore, J. Phys. B **32**, 4535 (1999).
[24] N. V. Vitanov, T. Halfmann, B. W. Shore, and K. Bergmann, Annu. Rev. Phys. Chem. **52**, 763 (2001).
[25] M. Shapiro and P. Brumer, Phys. Rep. **425**, 195 (2006).
[26] C. P. Lin, J. Bates, J. T. Mayer, and W. S. Warren, J. Chem. Phys. **86**, 3750 (1987).
[27] R. Uberna, Z. Amitay, R. A. Loomis, and S. R. Leone, Faraday Discuss. **113**, 385 (1999).
[28] Z. Amitay, R. Kosloff, and S. R. Leone, Chem. Phys. Lett. **359**, 8 (2002).

[29] J. B. Ballard, A. N. Arrowsmith, L. Huwel, X. C. Dai, and S. R. Leone, Phys. Rev. A **68**, 043409 (2003).
[30] J. Vala, Z. Amitay, B. Zhang, S. R. Leone, and R. Kosloff, Phys. Rev. A **66**, 062316 (2002).
[31] R. S. Judson and H. Rabitz, Phys. Rev. Lett. **68**, 1500 (1992).
[32] C. J. Bardeen, V. V. Yakovlev, K. R. Wilson, S. D. Carpenter, P. M. Weber, and W. S. Warren, Chem. Phys. Lett. **280**, 151 (1997).
[33] V. D. Kleiman, S. M. Arrivo, J. S. Melinger, and E. J. Heilweil, Chem. Phys. **233**, 207 (1998).
[34] T. Witte, T. Hornung, L. Windhorn, D. Proch, R. de Vivie-Riedle, M. Motzkus, and K. L. Kompa, J. Chem. Phys. **118**, 2021 (2003).
[35] T. Witte, J. S. Yeston, M. Motzkus, E. J. Heilweil, and K. L. Kompa, Chem. Phys. Lett. **392**, 156 (2004).
[36] C. Ventalon, J. M. Fraser, M. H. Vos, A. Alexandrou, J. L. Martin, and M. Joffre, Proc. Natl. Acad. Sci. U.S.A. **101**, 13216 (2004).
[37] D. J. Maas, D. I. Duncan, A. F. G. van der Meer, W. J. van der Zande, and L. D. Noordam, Chem. Phys. Lett. **270**, 45 (1997).
[38] D. J. Maas, D. I. Duncan, R. B. Vrijen, W. J. van der Zande, and L. D. Noordam, Chem. Phys. Lett. **290**, 75 (1998).
[39] D. J. Maas, M. J. J. Vrakking, and L. D. Noordam, Phys. Rev. A **60**, 1351 (1999).
[40] F. Eickemeyer, R. A. Kaindl, M. Woerner, T. Elsaesser, and A. M. Weiner, Opt. Lett. **25**, 1472 (2000).
[41] T. Witte, D. Zeidler, D. Proch, K. L. Kompa, and M. Motzkus, Opt. Lett. **27**, 131 (2002).
[42] T. Witte, K. L. Kompa, and M. Motzkus, Appl. Phys. B: Lasers Opt. **76**, 467 (2003).
[43] H. S. Tan and W. S. Warren, Opt. Express **11**, 1021 (2003).
[44] N. A. Naz, H. S. S. Hung, M. V. O'Connor, D. C. Hanna, and D. P. Shepherd, Opt. Express **13**, 8400 (2005).
[45] M. Tsubouchi and T. Momose, J. Opt. Soc. Am. B **24**, 1886 (2007).
[46] R. A. Kaindl, M. Wurm, K. Reimann, P. Hamm, A. M. Weiner, and M. Woerner, J. Opt. Soc. Am. B **17**, 2086 (2000).
[47] S. H. Shim, D. B. Strasfeld, E. C. Fulmer, and M. T. Zanni, Opt. Lett. **31**, 838 (2006).
[48] S. H. Shim, D. B. Strasfeld, and M. T. Zanni, Opt. Express **14**, 13120 (2006).
[49] C. Gollub, U. Troppmann, and R. de Vivie-Riedle, New J. Phys. **8**, 48 (2006).
[50] C. M. Tesch, L. Kurtz, and R. de Vivie-Riedle, Chem. Phys. Lett. **343**, 633 (2001).
[51] C. M. Tesch and R. de Vivie-Riedle, Phys. Rev. Lett. **89**, 157901 (2002).
[52] U. Troppmann, C. M. Tesch, and R. de Vivie-Riedle, Chem. Phys. Lett. **378**, 273 (2003).
[53] C. M. Tesch and R. de Vivie-Riedle, J. Chem. Phys. **121**, 12158 (2004).
[54] U. Troppmann and R. de Vivie-Riedle, J. Chem. Phys. **122**, 154105 (2005).
[55] B. M. R. Korff, U. Troppmann, K. L. Kompa, and R. de Vivie-Riedle, J. Chem. Phys. **123**, 244509 (2005).
[56] D. Babikov, J. Chem. Phys. **121**, 7577 (2004).
[57] T. Momose, H. Hoshina, M. Fushitani, and H. Katsuki, Vib. Spectrosc. **34**, 95 (2004).
[58] T. Momose, M. Fushitani, and H. Hoshina, Int. Rev. Phys. Chem. **24**, 533 (2005).
[59] J. P. Toennies and A. F. Vilesov, Angew. Chem., Int. Ed. **43**, 2622 (2004).
[60] F. Stienkemeier and K. K. Lehmann, J. Phys. B **39**, R127 (2006).
[61] M. Tsubouchi and T. Momose (to be published).
[62] J. M. Brown, A. R. H. Cole, and F. R. Honey, Mol. Phys. **23**, 287 (1972).
[63] M. Mizushima, Phys. Rev. A **5**, 143 (1972).
[64] A. W. Mantz, J. P. Maillard, W. B. Roh, and K. N. Rao, J. Mol. Spectrosc. **57**, 155 (1975).
[65] D. Goorvitch and C. Chackerian, Astrophys. J., Suppl. Ser. **91**, 483 (1994).
[66] J. O. Hirschfelder, C. F. Curtis, and R. B. Bird, *Molecular Theory of Gases and Liquids* (Wiley, New York, 1954).
[67] J. Danielak, U. Domin, R. Kępa, M. Rytel, and M. Zachwieja, J. Mol. Spectrosc. **181**, 394 (1997).
[68] F. P. Billingsley II, J. Mol. Spectrosc. **61**, 53 (1976).
[69] P. Bundgen, A. J. Thakkar, A. Kumar, and W. J. Meath, Mol. Phys. **90**, 721 (1997).
[70] S. A. C. McDowell and W. J. Meath, Can. J. Chem. **76**, 483 (1998).
[71] P. M. Felker and A. H. Zewail, J. Chem. Phys. **86**, 2460 (1987).
[72] J. S. Baskin, P. M. Felker, and A. H. Zewail, J. Chem. Phys. **86**, 2483 (1987).